Limnol. Oceanogr., 54(1), 2009, 145–159

Increases in the longwave photobleaching of chromophoric dissolved organic matter in coastal waters

Christopher L. Osburn[1,2]
Marine Biogeochemistry Section, Code 6114, Naval Research Laboratory, Washington, District of Columbia 20375

Daniel W. O'Sullivan
Department of Chemistry, US Naval Academy, Annapolis, Maryland 21402

Thomas J. Boyd
Marine Biogeochemistry Section, Code 6114, Naval Research Laboratory, Washington, District of Columbia 20375

Abstract

Salinity effects on the photobleaching of chromophoric dissolved organic matter (CDOM) due to coastal mixing were investigated through a comparative study of surrogate and surface-water CDOM. Suwannee River humic acid (SRHA) and ultrafiltered river dissolved organic matter (UDOM) added to mixtures of river and seawater permeates (<1 kDa) that varied in salinity from 0 to 33 to mimic coastal mixing. Surface-water CDOM was collected from the Chesapeake Bay in January, June, and September 2002. Shortwave CDOM absorption loss (e.g., 280 nm) did not change with salinity; however, longwave CDOM absorption loss (e.g., 440 nm) often decreased by 10% to 40% with salinity. Apparent quantum yields for average absorption loss from 280 to 550 nm (φ_{avg}) increased with salinity for both surrogate and surface-water CDOM, providing evidence for an effect of salinity independent of light absorption among different samples. Further, hydrogen peroxide photoproduction from UDOM increased from 15 to 368 nmol L^{-1} h^{-1} with salinity, even though pH values were circumneutral. A kinetic model demonstrated that, at circumneutral pH and iron concentrations expected for the Chesapeake Bay, photo-Fenton chemistry could not explain the increase in hydrogen peroxide production quantum yields (φ_{hp}) with salinity. Using φ_{avg} for the SRHA and UDOM surrogates, a model of the change in surface-water CDOM photoreactivity in the Chesapeake Bay as a function of salinity suggested additional CDOM inputs for the lower Chesapeake Bay. Because estuarine mixing increases photobleaching of longwave CDOM absorption, the modeling of absorption coefficients above 400 nm may underestimate dissolved organic matter in coastal waters.

One of the most important factors controlling light transmission in coastal waters is absorption by chromophoric dissolved organic matter (CDOM). As a control, CDOM affects ocean color and structures the underwater light environment for photosynthesis and aquatic photochemistry (Neale and Kieber 2000). Subsequently, light absorption by CDOM initiates numerous photochemical reactions ultimately resulting in loss of CDOM absorption, or photobleaching. Sunlight photobleaching is an important CDOM removal mechanism in surface waters of the coastal ocean (Miller and Zepp 1995; Vodacek et al. 1997), yet the physicochemical conditions that govern CDOM photoreactivity are poorly understood.

CDOM photoreactivity is not static. Del Vecchio and Blough (2002) found a decrease in efficiency of direct and indirect photobleaching with increasing wavelengths, yet greater relative photobleaching at longer wavelengths. Moreover, CDOM photobleaching is a function of iron availability and photochemistry (Gao and Zepp 1998; White et al. 2003). Osburn and Morris (2003) suggested that CDOM photoreactivity can increase with salinity across an estuarine gradient, but Minor et al. (2006) found a decrease in CDOM photobleaching at 280 nm when humic CDOM was added to an artificial salinity gradient used to mimic coastal mixing. Although many studies have investigated factors controlling CDOM photoreactivity, discrepancies in results can arise from different metrics used to define CDOM photoreactivity (Hu et al 2002). Given the influence of CDOM on surface-water carbon cycling, it is important to understand the controls on its photoreactivity in a consistent manner.

CDOM is comprised largely of humic substances (HS) of terrestrial origin. Emerging paradigms of the nature of HS (Sutton and Sposito 2005) are changing views of its underlying properties, such as ultraviolet-visible absorption, and ultimately its photoreactivity (Del Vecchio and

[1] Corresponding author (chris_osburn@ncsu.edu).
[2] Current address: Department of Marine, Earth, and Atmospheric Sciences, North Carolina State University, Raleigh, North Carolina 27695.

Acknowledgments

We thank Mike Montgomery, Duane Meek, and Joe Smith for help with field sampling. Richard Coffin and Linda Chrisey provided financial support. Patrick Neale provided access to the solar simulator. Braden Giordano and three anonymous reviewers provided helpful comments on this manuscript. Special thanks to the captain and crew of the R/V *Cape Henlopen* for providing logistical support.

This research was funded in part by Office of Naval Research Work Unit MA013-01-44-8541 and by a National Research Council postdoctoral fellowship award to C.L.O. The opinions and assertions contained herein are not to be construed as official or reflecting the views of the U.S. Navy.

Blough 2004). CDOM absorption as measured by ultraviolet-visible spectrophotometry displays a featureless exponential decay with increasing wavelength. The nature of this absorption has been the focus of some debate because CDOM, as an optical component of dissolved organic matter (DOM), is difficult to characterize, being comprised of many different molecules. Recent work by Del Vecchio and Blough (2002, 2004) has elucidated the probable chemistry behind the light absorption of HS, i.e., the chemistry behind CDOM absorption. They proposed a model of donor–acceptor charge transfer that produces a featureless spectrum and is much more widely applicable across systems than models of superposition of multiple chromophores (Korshin et al 1997; Goldstone et al 2004). Thus, the spectral feature of CDOM must be summarized and studied to adequately address the reactivity of CDOM. This point is especially critical when considering the polychromatic, variable nature of sunlight.

CDOM originating in terrestrial environments transits through rivers and estuaries onto coastal shelves, experiencing large changes in ionic composition and physicochemical environment, yet is generally conservative. If the changing physicochemical environment causes some disruption in intramolecular charge transfer by altering the proximity or conformation of the molecular features involved in the charge transfer, then we would expect to see an effect in long-wavelength (>350 nm) absorption, rather than an effect at shorter wavelengths (e.g., 280 or 350 nm). Further, CDOM photobleaching in the blue (>400 nm) might complicate retrievals of absorption from remote sensing data and underestimate terrestrial DOM flux in the coastal ocean.

The goal of this study was to determine the effect of coastal mixing on CDOM photoreactivity by examining the spectral nature of photobleaching and investigating its variability along a salinity gradient. Based on results published elsewhere (Osburn and Morris 2003; Boyd and Osburn 2004) we hypothesized that CDOM photobleaching reactions are more efficient in high-ionic-strength solutions such as seawater and would lead to an increase in the apparent quantum yield (AQY). Although we did not investigate specific chemical reactions occurring from sunlight exposure, we quantified the effect of salinity using changes to the optical properties of river DOM in controlled experiments coupled with field observations along a salinity gradient.

Methods

Sample collection and handling—Water samples used in experiments reported here were collected aboard the R/V *Cape Henlopen* in the Chesapeake Bay (CB), in January, June, and September of 2002. For each cruise, we sampled a minimum of three stations along axial transects in the CB and Middle Atlantic Bight (MAB; Fig. 1). Salinity (S) was determined according to the practical salinity scale (PSS 1978) from the ship's flow-through system and conductivity–temperature sensors (CTD). We collected samples over a salinity range of 0–34. The location of each station for each sampling date and relevant optical and chemical information are provided in Table 1. Dissolved organic carbon (DOC) concentrations were measured by high-temperature oxidation on an MQ1001 Total Organic Carbon analyzer with modifications following Boyd and Osburn (2004). Average DOC concentration and standard deviation on duplicates are reported (Table 1).

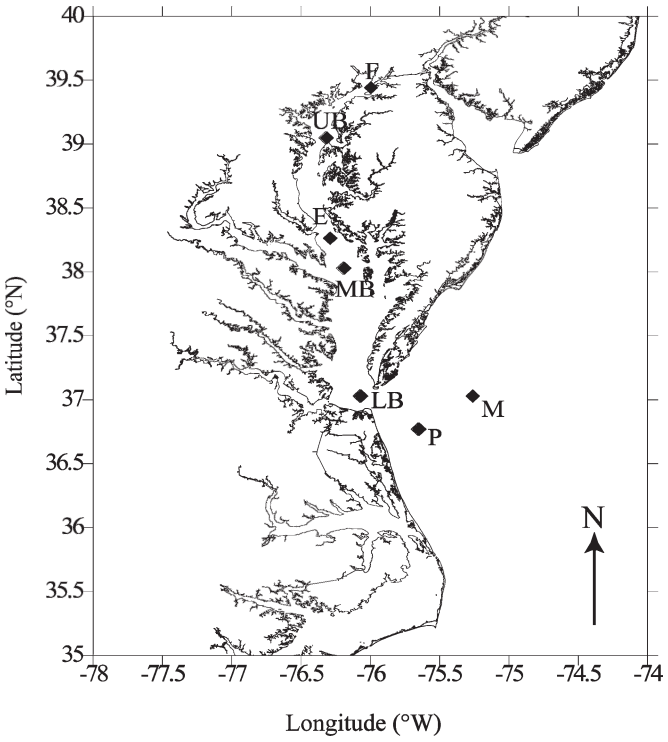

Fig. 1. The sample collection sites in the CB and MAB used in this study.

Water samples were collected in 20-liter Niskin bottles (General Oceanics) affixed to a Seabird CTD rosette at depths to minimize prior light exposure. Usually, sample collection was at a depth just below the pycnocline or at a depth below the deepest penetration of photosynthetically active radiation (450–700 nm) when we were able to measure light transmission (in January 2002, Sta. M was sampled at night). Water samples were immediately serial-filtered through 3-μm and 0.2-μm polyethersulfone (PES) filters (Pall Life Sciences) into 20-liter acid-washed, autoclaved polycarbonate carboys. All filters were flushed with MilliQ-grade laboratory water and with sample before the carboys were filled. Aliquots were collected for measurement of absorbance and DOC concentration. Samples were kept at ambient temperature in the dark until further processing.

Within 4 h of collection, the samples were ultrafiltered using a tangential flow filtration (TFF) system with polyethersulfone membrane having a nominal cutoff of 1 kDa (Separation Engineering). Tangential flow ultrafiltration separates pre-filtered DOM into a high-molecular-weight fraction (ultrafiltered river dissolved organic matter [UDOM]) and a low-molecular-weight (LMW) fraction (permeate), which was reserved for photobleaching experiments. A concentration factor of greater than 40 : 1 was

Table 1. Measurements from shipboard sampling for samples used in this study. Station codes are: M, offshore marine; E, mid-salinity estuarine; F, Susquehanna River freshwater; P, bay plume; LB, lower-bay polyhaline; MB, mid-bay mesohaline; UB, upper bay oligohaline. Data are from replicate hydrocasts at the indicated sampling depth; these were also the depths at which water was collected and processed for UDOM separation by TFF and used in subsequent experiments. The pH data were obtained from the Chesapeake Bay Program water quality database (http://www.chesapeakebay.net/wquality.htm).

Sampling	Station code	Position		Sampling depth (m)	Salinity	Temperature (°C)	pH	Dissolved Fe (μmol L^{-1})	a_{350} (m^{-1})	DOC* (μmol C L$^{-1}\pm$SD)
		Latitude (°N)	Longitude (°W)							
Jan 2002	M	37°05.49′	75°30.97′	21.1	33.9	9.6	8.1	<0.02†	0.6	102±9
	E	38°34.08′	76°26.30′	8.4	18.3	5.7	7.7	n.d.‡	1.5	402±8
	F	39°26.51′	75°59.89′	5.4	2.3	5.4	7.6	0.10‡	1.96	213±18
Jun 2002	M	37°05.44′	75°31.03′	9.5	33.1	20.1	8.1	<0.02†	0.63	121±15
	P	36°59.93′	75°56.33′	3	28.9	21.4	8.1	<0.02†	1.62	—
	E	38°14.53′	76°17.63′	5.9	13.9	22.1	8.3	n.d.‡	1.73	312±13
	F	39°25.40′	76°01.96′	3	0.1	23.7	7.2	0.10‡	2.49	203±8
Sep 2002	M	37°05.34′	75°31.26′	2	32.1	23.4	8.2	<0.02†	0.47	112±10
	P	36°56.93′	75°56.33′	2.1	28.4	24	8.1	—	0.99	123±5
	LB	37°01.30′	76°30.80′	1.6	24.4	24.9	8.1	—	1.57	207±13
	MB	38°06.94′	76°16.09′	1.9	17.2	24.7	7.8	—	1.62	178±6
	E	38°25.99′	76°22.75′	1.7	16.2	24.9	7.9	n.d.‡	1.5	177±8
	UB	39°18.94′	76°12.56′	1.9	11.7	24.6	7.6	0.21‡	2.06	187±4
	F	39°26.82′	76°01.46′	1.7	6.4	25.2	7.1	0.10‡	2.81	198±3

* DOC, dissolved organic carbon.
† Data are from B. Lewis (unpubl.).
‡ Data are from Skrabal (1995) for similar sampling locations and salinities; n.d., not detected.

obtained for each of the samplings. Mass balance calculations for the processing of freshwater by TFF were 102% for DOC recovery and 99% for CDOM absorption at 350 nm. The TFF system was cleaned following the procedures in Boyd and Osburn (2004), so that DOC concentration in the blanks for the system were <25 μmol L^{-1}. After the isolation procedure, both the UDOM and the permeate from each station were refiltered using 0.2-μm pore size sterile filter units (Millipore) and stored in the dark at 4°C until used in experiments.

CDOM photobleaching protocols—Two surrogates for terrigenous DOM were added to artificially created salinity gradients in separate photobleaching experiments. The DOM surrogates were Suwannee River humic acid (SRHA) and Susquehanna River UDOM. For the SRHA experiment, 2.0 mg of the humic acid was added in powdered form to LMW TFF permeate from offshore, mid-bay, and freshwater (near Turkey Point). For the UDOM experiment, 375 mL of UDOM (DOC concentration = 1999 μmol L^{-1}) was added to a mixture of the seawater and freshwater permeates, following Boyd and Osburn (2004). The mixture of UDOM with freshwater permeate represented a positive control. After preparation, each solution was re-filtered through 0.2-μm PES filters into sterile culture units. We did not observe any flocculation of humics while preparing our solutions or note any adhesion of humic material to the walls of the quartz bottles used in the experiments. The permeate CDOM absorption was always <10% of the final mixture (Table 2).

In separate photobleaching experiments, surface water collected from the CB was used without DOM surrogate addition. Surface water was collected during each of the January, June, and September cruises. The results of these experiments were then compared to the freshwater DOM surrogate experiments.

All photobleaching experiments were carried out in 125-mL acid-washed quartz bottles (4 cm wide × 15 cm long) that had been thoroughly washed and precombusted at 550°C for at least 6 h. After re-filtering, samples were carefully transferred to the 125-mL quartz bottles and capped with ground glass stoppers without headspace. The caps were then wrapped in Parafilm, taking care not to obscure the quartz portion of the bottle's body.

Experiments were conducted on the roof of the Naval Research Laboratory Chemistry building in a flow-through water bath to buffer temperature and exposed to ambient sunlight for periods of 2–3 d. The depth of the water was regulated so that a thin (2–5 cm) layer of water covered the samples. Absorption measurements of this overlying water revealed that absorption at wavelengths >300 nm was less that 5% of the sample absorption. For most exposures, we performed light and dark treatments in triplicate. One

Table 2. Initial CDOM absorption values for the initial mixture and permeate at salinities used in the experiments with Suwannee River humic acid (SRHA) and ultrafiltered river DOM (UDOM).

Experiment	Salinity	Initial a_{350} of mixture (m^{-1})	a_{350} of permeate (m^{-1})
SRHA	33.1	5.83	0.15
	14.1	6.08	0.35
	0.8	6.00	0.67
UDOM	22.5	5.98	0.35
	11.7	5.47	0.30
	6.3	5.44	0.33
	3.6	5.41	0.37
	0.9	5.27	0.42

experiment, using Sta. F surface water from June 2002, was performed using a solar simulator with different irradiation geometry than the natural sunlight exposures. Details of the experimental design using the solar simulator are given in O'Sullivan et al. (2005). Absorption measurements were conducted within 24 h of the end of each experiment.

For the UDOM experiment, bottles were retrieved at 5, 10, and 19 h for measurement of CDOM absorption and hydrogen peroxide concentration. Hydrogen peroxide analyses using a high-performance liquid chromatography (HPLC) technique (Lee et al. 1995) were modified slightly for work in seawater by addition of methanol (O'Sullivan et al. 2005). A mobile phase composition of 95% 1.00×10^{-3} mol L^{-1} H_2SO_4 and 5% methanol was used for the analysis. The source and concentrations of reagents, the synthesis of standards, the stability of H_2O_2 along a salinity range of 0–33 and the HPLC parameters are described in detail in O'Sullivan et al. (2005). The average precision was better than ±8% for analysis of the hydroperoxides in this study. The detection limit for H_2O_2 was 3.0×10^{-8} mol L^{-1}, defined as three times the standard deviation of the blank. No short-chain organic peroxides were observed above the detection limit of 1.5×10^{-8} mol L^{-1} in this study. The analytical system was calibrated daily using standard solutions prepared in MilliQ water. Standard additions of H_2O_2 and methylhydroperoxide to waters having salinities from 0 to 34 and a variety of DOC concentrations exhibit the same response with the HPLC method. Separation of the peroxides from the sea salts and components of DOC on the HPLC column prior to the analytical reaction and fluorescence determination eliminated the need to perform standard additions for each analysis to account for matrix effects.

Natural and artificial sunlight exposure experiments were generally performed within 2 weeks of sample collection and processing, as dictated by clear weather conditions. All sample handling and processing was the same regardless of the exposure system. Ambient solar radiation during each exposure experiment was measured at four discrete channels (308, 320, 340, and 380 nm) using a Biospherical PUV-501 radiometer. Post-processing of the data involved quantifying the total irradiance (in μW cm^{-2} nm^{-1}) during each experiment and then recomputing the cumulative solar spectrum for each day using a Microsoft Excel spreadsheet model (Osburn et al. 2001). This model's input parameters were average daily ozone for the experiment and the daily integrated irradiance values obtained from the PUV-501. A numerical adjustment fitting parameter for longwave UV was optimized to reduce the residuals at 340 and 380 nm. The UV-B channel fits at 308 and 320 nm were further interpolated to provide the best fit to the measured data. The model was initially calibrated against measurements made with a spectroradiometer (Morris and Hargreaves 1997). The representative solar spectra were obtained from RT95 software (now RTBasic) from Biospherical Instruments. Total column ozone values for each experiment were obtained from the NASA website (http://toms.gsfc.nasa.gov/teacher/ozone_overhead.html). The irradiance values were then converted to mol photons m^{-2}.

O'Sullivan et al. (2005) describe irradiance measurement for the solar simulator design. Briefly, a spectroradiometer was used to measure lamp output from 280 to 600 nm. The resulting irradiance spectrum was summed over the 5-h exposure period. This amounts to approximately 5 h of light intensity at solar noon. Irradiance measurements from the PUV radiometer–based model or the spectroradiometer were then converted to mol photons m^{-2} nm^{-1} for later calculations.

CDOM measurements—Spectral absorbance of filtered water samples and of surrogate CDOM solutions was measured in 1-, 5-, and 10-cm quartz cells on either a HP8453 diode array spectrophotometer, a Hitachi U3000 scanning spectrophotometer, or a Shimadzu UV1601 scanning spectrophotometer. About 2% variation in replicate measurements of CDOM spectra was observed between these instruments. Measurements were made against air (empty cell holder) and the absorbance of 18 MΩ MilliQ water was subtracted from each sample spectrum. Raw absorbance values per nm, $A(\lambda)$ (AU), were measured from 250 to 750 nm and converted to absorption coefficients ($a(\lambda)$, in m^{-1}), according to the following relationship:

$$a(\lambda) = \frac{2.303 \times A(\lambda)}{L} \quad (1)$$

where L is the pathlength of the quartz cell and 2.303 converts from the natural logarithm. Following Stedmon et al. (2000), we corrected for baseline drifts, temperature effects, colloidal (<0.2 μm) scattering, or heterogeneity between the three spectrophotometers by fitting the following equation to calculated absorption coefficients from 280 to 550 nm:

$$a(\lambda) = a(\lambda)_0 \times e^{S_g(375 - \lambda)} + K \quad (2)$$

where λ is the wavelength (nm), λ_0 is the absorption coefficient at 375 nm, and S_g is the spectral slope coefficient of the absorption spectrum (in μm^{-1}). This procedure was necessary to account for the noise in absorbance spectra of Sta. M and the permeate samples at wavelengths above 400 nm where absorbance was low. The K value was used solely to adjust calculated $a(\lambda)$ in the nonlinear fit. The K value was not subtracted from absorption coefficients when they were recomputed using the fit parameters. All nonlinear fits used to calculate S_g had $r^2 > 0.95$ over the wavelength range 280 to 550 nm.

Computation of apparent quantum yields—The photoreactivity of CDOM in our experiments was measured as the AQY, defined as the average decrease in the absorption coefficient divided by the total mol photons absorbed m^{-2}, over the 280- to 550-nm waveband. The average decrease in CDOM absorption (Δa_{avg}) was defined as:

$$\Delta a_{avg} = \frac{\sum_{\lambda = 280}^{550} a(\lambda)_{initial} - a(\lambda)_{final}}{270} \quad (3)$$

Table 3. Results of 2–4 d sunlight exposures of surrogate CDOM and surface-water CDOM show distinct changes to absorption properties. Absorption losses (Δa_λ=final−initial) at 280, 350, and 440 nm, along with average absorption loss (280–500 nm), are reported with increases in spectral slope coefficient (ΔS_g), and mol photons absorbed (I_a). Averages and standard error of the mean (SEM) are shown for triplicates.

Experiment	Salinity	Δa_{280} (m^{-1})	SEM	Δa_{350} (m^{-1})	SEM	Δa_{440} (m^{-1})	SEM	Δa_{avg} (m^{-1})	SEM	ΔS_g (μm^{-1})	SEM	I_a (mol photons m^{-2})	SEM
SRHA	33.2	−2.18	0.03	−2.02	<0.01	−1.23	0.01	−1.62	0.02	3.02	0.05	13.39	0.06
	14.5	−2.33	0.09	−1.95	0.04	−1.06	0.02	−1.54	0.04	2.70	0.04	14.48	0.09
	0.8	−2.33	0.02	−1.63	<0.01	−0.79	0.01	−1.29	0.01	1.84	0.04	14.51	0.02
UDOM	22.5	−3.75	0.12	−1.33	0.02	−0.59	0.01	−1.04	0.02	1.54	0.07	25.49	0.01
	11.7	−4.30	0.10	−1.11	0.06	−0.44	0.01	−0.90	0.04	0.98	0.05	24.35	0.02
	6.3	−4.07	0.20	−0.89	0.08	−0.43	0.01	−0.87	0.05	0.92	0.02	24.74	0.15
	3.6	−3.84	0.10	−0.96	0.04	−0.38	0.01	−0.78	0.03	0.82	0.01	24.15	0.06
	0.9	−3.67	0.01	−0.83	0.03	−0.34	0.01	−0.65	0.01	1.05	0.10	24.07	0.06
Jan 2002	33.9	−0.75	0.02	−0.28	0.01	−0.06	0.00	−0.19	0.01	3.45	0.34	2.64	0.02
CDOM	18.3	−1.55	0.12	−0.40	0.04	−0.09	0.01	−0.33	0.02	1.57	0.32	7.88	0.21
	2.3	−1.50	0.06	−0.53	0.01	−0.12	0.01	−0.35	0.01	1.19	0.22	7.03	1.58
Jun 2002	33.1	−0.85	0.03	−0.28	0.01	−0.04	0.00	−0.19	0.01	4.39	0.18	1.91	0.01
CDOM	28.9	−0.93	0.01	−0.52	0.01	−0.12	0.00	−0.31	0.01	3.47	0.11	5.82	0.04
	13.9	−1.01	0.03	−0.38	0.02	−0.08	0.01	−0.26	0.01	2.01	0.21	9.17	0.12
	0.1	−1.09	0.17	−0.64	0.02	−0.18	0.00	−0.38	0.02	2.05	0.17	21.4	0.03
Sep 2002	32.1	−0.37	0.04	−0.19	0.01	−0.04	0.00	−0.11	0.01	4.63	0.10	1.03	0.02
CDOM	28.4	−1.02	0.04	−0.41	0.01	−0.09	0.00	−0.27	0.01	3.35	0.02	2.26	0.03
	24.4	−1.29	0.09	−0.51	<0.01	−0.11	0.01	−0.33	0.01	2.63	0.29	3.78	0.03
	17.2	−1.33	0.01	−0.39	0.01	−0.08	0.01	−0.28	0.01	0.63	0.14	4.31	0.04
	16.2	−1.46	0.05	−0.52	0.03	−0.12	0.01	−0.35	0.03	1.48	0.17	4.72	0.08
	11.7	−1.83	0.08	−0.50	0.03	−0.10	0.01	−0.37	0.03	0.40	0.12	5.47	0.09
	6.4	−1.27	0.05	−0.37	0.05	−0.08	0.02	−0.27	0.04	0.08	0.19	8.34	0.14

where $a(\lambda)_{initial}$ is the initial absorption coefficient at wavelength, λ, corrected for the absorption of the dark controls, and $a(\lambda)_{final}$ is the final absorption coefficient after exposure. The total quanta (I_a, in mol photons m^{-2}) absorbed by the sample during an exposure was calculated as:

$$I_a = I_0(\lambda) \times \left(1 - e^{-a(\lambda)_{geo} \times L}\right) \quad (4)$$

where $I_0(\lambda)$ is the incident radiant flux (in mol photons m^{-2} s^{-1}) measured at the surface of the exposure system during an experiment, $a(\lambda)_{geo}$ is the geometric average of the initial and final absorption coefficients, and L is the pathlength of the quartz bottle, in meters (quartz bottles = 0.0355 m). Following Osburn et al. (2001), the geometric average of initial and final absorption was used as an estimation of the change in the absorption coefficient with exposure, which has been shown to decrease exponentially (Zepp 1988; Miller and Zepp 1995; Goldstone et al. 2004). Thus, the AQY for CDOM photobleaching is:

$$\vartheta_{avg} = \frac{\Delta a_{avg}}{I_a} \quad (5)$$

similar to O'Sullivan et al. (2005) and Tzortziou et al. (2007). We chose not to use molar absorptivity in our calculations because of the uncertainty of measuring exactly the chromophores that comprise CDOM (Miller 1998), thus AQY are not dimensionless and have the units "m (mol photons^{-1})". Integration of the absorbed mol photons over the time of exposure eliminated the units of seconds.

All statistical analyses were performed in the Matlab version 7.3 computing environment using the Statistics and Curve Fitting toolboxes.

Results

Effect of sunlight and salinity on CDOM properties—After 2–3 d sunlight exposure, all experimental treatments showed a loss of absorption, consistent with photobleaching of CDOM, producing negative changes in absorption coefficients and positive changes in S_g values (Table 3). Differences between dark controls and initial absorption measurements were not found be significant ($F_{21,22}$ = 1.023, p = 0.480, n = 22). The decrease in CDOM absorption at individual wavelengths was strongly correlated with initial CDOM absorption. For example, Δa_{350} was dependent on $a_{350,initial}$ (Pearson's correlation coefficient = −0.87, $p < 0.001$, n = 22). Thus, more photobleaching occurred at wavelengths having stronger initial absorption, and therefore most CDOM photobleaching was blue-shifted towards the UV wavelengths.

This effect generally was consistent among all samples and treatments and varied with wavelength (Fig. 2), but several exceptions were noted. First, in the SRHA addition experiment, photobleaching reached a plateau in magnitude (~2.2 m^{-1}) near 280 nm (Fig. 2A). A similar plateau in Δa was observed in the CB surface-water exposures at salinities of 28.9 (June 2002) and at salinities of 28.4 and 24.4 (September 2002). Second, in the surface-water

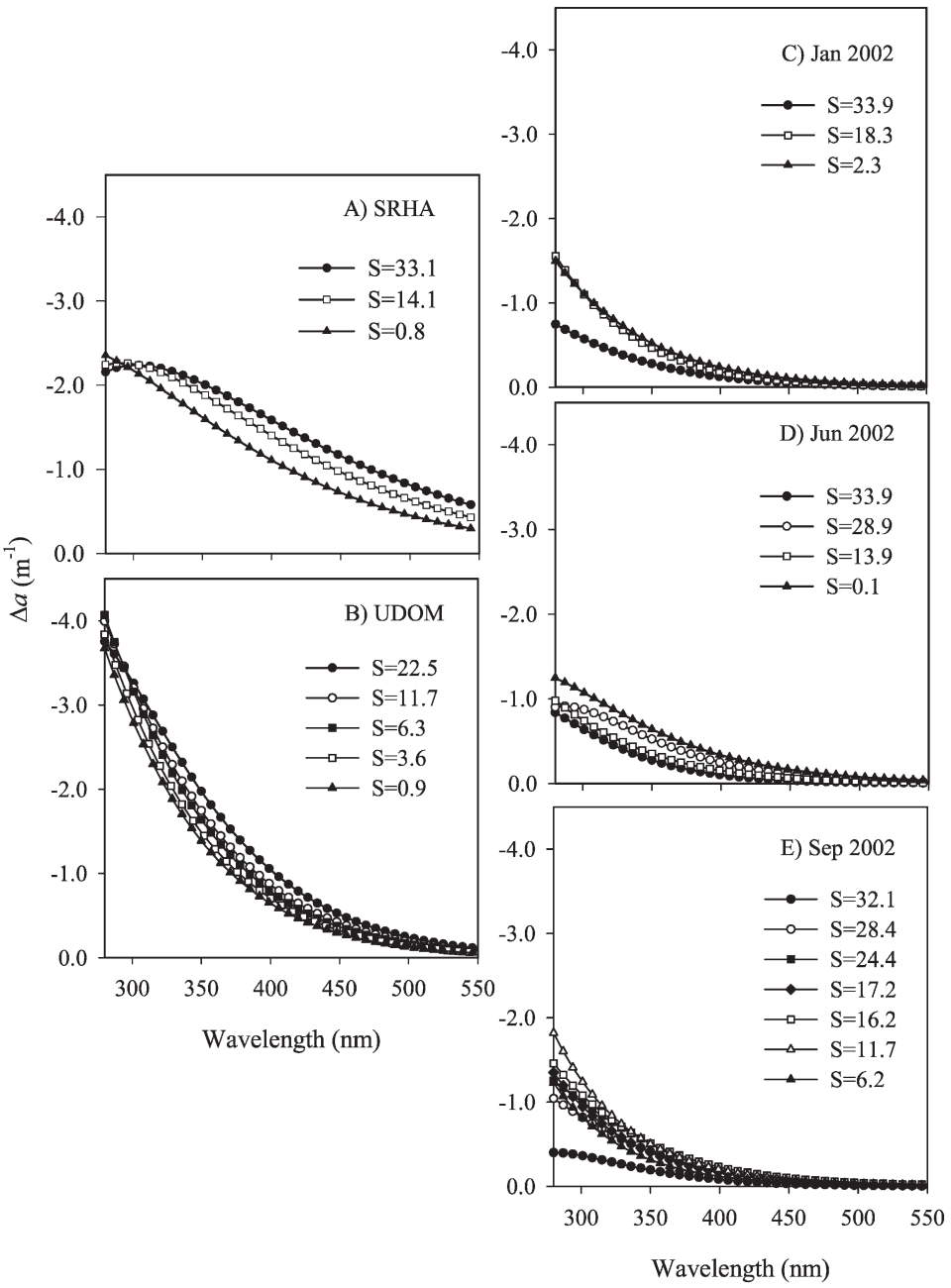

Fig. 2. Photobleaching measured as decreases in the absorption coefficient (Δa) per nm in sunlight exposures of (A) SRHA, (B) UDOM, and (C–E) surface-water CDOM. Each curve represents a different salinity (S), as indicated.

experiments, more absorption loss occurred in the short-wave region of the spectrum (<350 nm) in January and September 2002 than in June 2002 (Fig. 2C–E). Third, the separation of Δa spectra with salinity showed opposite patterns in the surface-water CDOM as compared to the surrogates. The Δa values increased when either surrogate was mixed into higher-salinity permeates, but generally decreased with increasing salinity for surface-water CDOM.

Light absorption (I_a) did not vary dramatically among experiments using either SRHA or UDOM as a CDOM surrogate (Table 3). For the SRHA experiment, I_a for the S = 33.9 treatment was significantly less than for both the S = 14.5 and S = 0.6 treatments ($p < 0.01$), which can be attributed to the lower absorption of the seawater permeate to which SRHA was added. By contrast, the S = 22.5 treatment in the UDOM experiment had roughly 6% greater mol photons absorbed than did the S = 0.9 treatment. The differences in light absorption likely reflect variation in preparing the solutions. However, surrogate CDOM light absorption was much greater than surface-water CDOM light absorption in most cases. In surface-

water experiments, light absorption decreased with salinity, but light absorption was not constant among stations over three samplings in 2002. Sta. F had the largest I_a (21.4 mol photons m^{-2}) in June 2002, approximating the light absorption of the UDOM treatments (Table 3). At 1.03 mol photons m^{-2}, Sta. M in September 2002 had the smallest I_a. In general I_a was greater for lower-salinity waters having higher CDOM absorption.

CDOM photobleaching in the exposures of SRHA and UDOM amendments was 2–20 times greater than in the exposures of surface water, with the greatest differences occurring at $\lambda < 350$ nm. Much less photobleaching (near the limit of detection) was observed at $\lambda > 450$ nm in the surface-water experiments for seawater samples (Fig. 2). CDOM photobleaching at 280 nm did not show a pattern with salinity for either CDOM surrogate (Table 3). In the SRHA experiment, the loss of absorption at 280 nm (Δa_{280}) was not significantly different among the salinity treatments (Bonferroni multiple comparisons test, $p = 0.135$, df = 6). Similarly, in the UDOM experiment, no significant difference in Δa_{280} was found among salinity treatments (Bonferroni multiple comparisons test, $p = 0.067$, df = 9).

Differences in photobleaching measured at single wavelengths among surrogate CDOM treatments were apparent and began to show some correlation with salinity. In the SRHA experiment, Δa_{350} and Δa_{440} both increased by $\sim$0.40 m^{-1} when SRHA was added to seawater permeate (S = 33.2). Similarly, in the UDOM experiment, Δa_{350} increased by 0.50 m^{-1} and Δa_{440} by 0.30 m^{-1} when UDOM was added to permeate at S = 22.5 compared to UDOM added to freshwater permeate (S = 0.9).

Salinity did not increase the photobleaching at individual wavelengths for CB surface waters in 2002. Rather, Δa decreased as salinity increased in exposure experiments using CDOM from CB surface waters, an opposite trend from the surrogate CDOM experiments. Decreases in Δa with salinity were consistent for each of the three wavelengths presented in Table 3, though some variation did exist, particularly in the September 2002 transect, which included more sampling sites. In general, freshwater stations had larger decreases in Δa than did seawater stations. The shortwave response to photobleaching seemed most variable, because the difference between freshwater and seawater Δa_{280} was 0.75 m^{-1} in January, decreased to 0.24 m^{-1} in June, then increased to 1.46 m^{-1} in September (Table 3).

The effect of salinity on Δa_{avg} followed the same pattern as Δa for individual absorption coefficients. Δa_{avg} generally increased with salinity in the SRHA and UDOM experiments, yet decreased with salinity in the surface-water CDOM experiments (Table 3). However, the trend was only significant for the UDOM surrogate (Fig. 3A). When all surrogate and surface-water CDOM results were combined, Δa_{avg} was significantly related to Δa_{350} ($r^2 = 0.99$, $p < 0.001$, $n = 21$). Therefore, Δa_{avg} was similar in magnitude to a wavelength used in many other photobleaching studies and can be useful in comparison with other results.

Changes to spectral slope (ΔS_g) were also evident in the CDOM exposures, and the results were more uniform than absorption coefficients between surrogate and surface-water CDOM treatments. Spectral slope increased for all CDOM solutions exposed to sunlight, except for Sta. F in September 2002, in which the measured ΔS_g was not significantly different from zero (Table 3). In general there was about twice as much change to spectral slope in the seawater CDOM samples as there was in the riverine CDOM samples. The magnitude of difference in ΔS_g between the high-salinity and low-salinity treatments was $\sim$2 μm^{-1} for the SRHA surrogate and surface-water CDOM, but only 0.5 μm^{-1} for the UDOM surrogate. Spectral slope increased significantly with salinity for the SRHA experiment ($r^2 = 0.87$, $p < 0.001$, $F = 47.500$, df = 8, $n = 9$) and for the UDOM experiment ($r^2 = 0.68$, $p < 0.001$, $F = 27.176$, df = 14, $n = 15$). For surface-water CDOM, ΔS_g

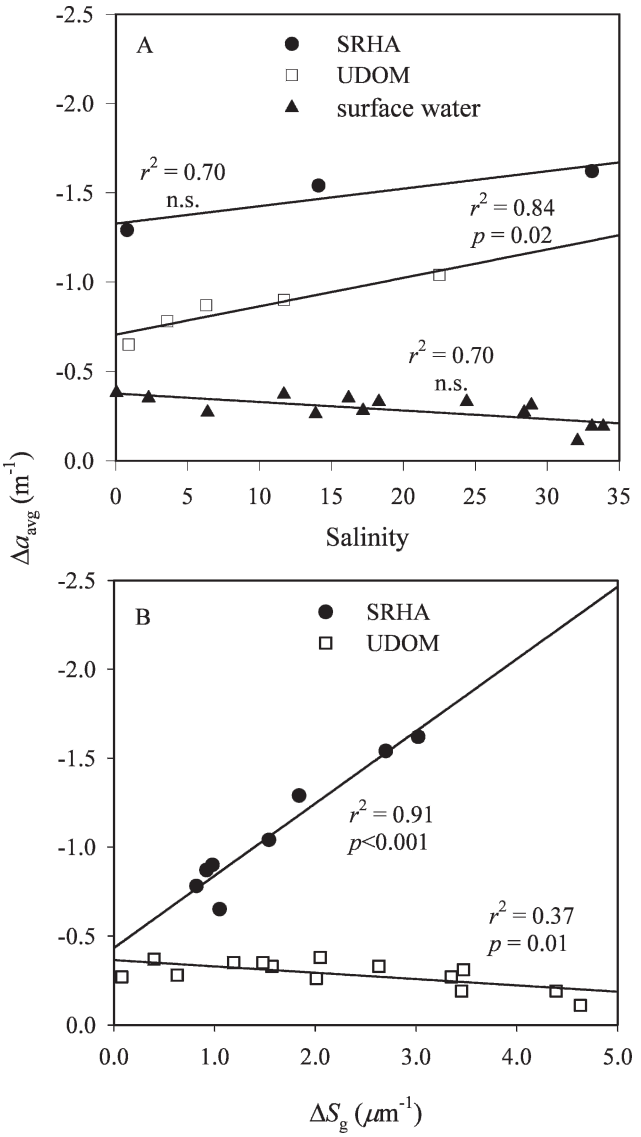

Fig. 3. The photobleaching averaged over the 280–550-nm waveband (Δa_{avg}) compared to (A) salinity and to (B) increases in the spectral slope coefficient, ΔS_g. Only the UDOM had a significant increase in Δa_{avg} with salinity. However, surrogate CDOM exhibited an increase in Δa_{avg} with ΔS_g. A decrease in Δa_{avg} with ΔS_g was found for the surface-water CDOM.

Table 4. Relative photobleaching ($\Delta a/a$) measured at 280, 350, and 440 nm.*

Experiment	Salinity	$\Delta a/a$(280)	$\Delta a/a$(350)	$\Delta a/a$(440)
SRHA	33.1	0.19	0.35	0.50
	14.1	0.19	0.33	0.47
	0.8	0.17	0.27	0.38
UDOM	22.5	0.12	0.20	0.31
	11.6	0.12	0.18	0.26
	6.3	0.12	0.17	0.24
	3.6	0.11	0.16	0.22
	0.9	0.10	0.15	0.20
Jan 2002 CDOM	33.9	0.31	0.43	0.56
	18.3	0.25	0.33	0.42
	2.3	0.20	0.27	0.34
Jun 2002 CDOM	33.1	0.24	0.43	0.61
	28.9	0.13	0.32	0.51
	13.9	0.15	0.25	0.36
	0.1	0.13	0.24	0.37
Sep 2002 CDOM	32.3	0.17	0.41	0.61
	28.4	0.26	0.41	0.57
	24.4	0.19	0.33	0.47
	17.2	0.21	0.25	0.30
	16.2	0.20	0.28	0.36
	11.7	0.22	0.24	0.27
	6.4	0.12	0.11	0.10

* SRHA, Suwannee River humic acid; UDOM, ultrafiltered river dissolved organic matter; CDOM, chromophoric dissolved organic matter.

also increased with salinity and the magnitude of ΔS_g was similar to the surrogates over a salinity range of 0–33.

The relationship between Δa_{avg} and ΔS_g for surrogate treatments exhibited an opposite trend when surrogates were compared to surface-water CDOM (Fig. 3B). For the surrogate CDOM group, a positive correlation between the loss of average absorption and the increase in S_g value was found ($r^2 = 0.91$, $p < 0.001$, $n = 8$). A negative correlation was found between Δa_{avg} and ΔS_g for the surface-water CDOM group, and although the correlation was significant, it was weaker than for the surrogate CDOM ($r^2 = 0.37$, $p = 0.012$, $n = 14$).

Relative changes in CDOM photobleaching with salinity—The relative photobleaching was not constant across all wavelengths and illustrated the effect of salinity on longwave CDOM absorption >350 nm as opposed to shortwave absorption <350 nm. Relative photobleaching is the change in CDOM absorption per nm after photobleaching divided by the initial absorption per nm, $\Delta a/a$ (Tzortziou et al. 2007):

$$\Delta a/a = \frac{a(\lambda,\text{initial}) - a(\lambda,\text{final})}{a(\lambda,\text{initial})} \quad (6)$$

At 280 nm, $\Delta a/a$ did not change substantially with salinity for the SRHA and UDOM treatments, but showed an increase with salinity for the surface-water experiments (Table 4). Relative photobleaching at 350 and 440 nm was always greater in value than at 280 nm. The differences in $\Delta a/a$ are most pronounced when viewing the entire 280–550 waveband (Fig. 4). Near 280 nm, relative photobleaching was about 0.10 (roughly 10% at that wavelength) and increased with decreasing wavelength. Beyond 350 nm, the separation of each relative photobleaching spectrum by salinity is apparent. Into the blue region (>400 nm), SRHA had $\Delta a/a$ values of 0.25 at S = 0.9, increasing to 0.35 at S = 33.2. A larger effect was seen in the UDOM experiment, where $\Delta a/a$ ranged from 0.20 to nearly 0.40 at 550 nm (Fig. 4A,B).

In the surface-water CDOM experiments, $\Delta a/a$ spectra showed the same trend as for the surrogate CDOM (Fig. 4C–E). The amount of relative photobleaching was much greater for surface-water CDOM than for the surrogate CDOM. For example, at 280 nm, the range of $\Delta a/a$ values for all salinities in each of the three cruises was 0.10–0.30. However, at 550 nm, most offshore sites in the MAB experienced nearly a 70% decrease in absorption coefficient ($\Delta a/a \sim 0.70$). The freshwater end-members had lower $\Delta a/a$ (0.10 to 0.30). Thus, the relative amount of photobleaching was greater for longwave CDOM absorption than for shortwave CDOM absorption, and salinity appeared to increase the effect of longwave photobleaching.

Effect of salinity on CDOM photoreactivity—Similar to relative absorption losses, the efficiency of absorption loss, measured as φ_{avg}, in surrogate and surface-water CDOM was influenced by changes in salinity. The calculation of apparent quantum yields normalized Δa_{avg} to light absorption, i.e., the energy that could cause photobleaching. Therefore, the photoreactivity of solutions having a wide range of light absorption could be compared.

AQY calculations revealed a strong dependence of photobleaching efficiency on salinity (Table 5). The value of φ_{avg} increased by 35% and 25% between low- and high-salinity treatments for both CDOM surrogates, and φ_{avg} calculated for the SRHA surrogate was 2–3 times larger than for the riverine UDOM surrogate. Surface-water φ_{avg} exhibited larger increases with salinity than did the surrogates. During 2002, the increases in φ_{avg} calculated from surface-water CDOM exposures to sunlight were 52%, 82%, and 71% for January, June, and September, respectively.

Linear regression models of φ_{avg} vs. salinity were calculated for each surrogate and surface-water CDOM experiment (Table 5). Each linear regression was significant ($p < 0.05$), and its slope provided a comparative term for the degree to which φ_{avg} changed with salinity. The SRHA surrogate had the largest r^2 value, whereas the January 2002 surface-water CDOM had the lowest r^2 (0.64). Pooling the surface-water CDOM φ_{avg}, the linear model remained significant, but the correlation was lower ($r^2 = 0.29$, $p = 0.003$, $n = 25$):

$$\varphi_{avg} = 20.33 \times 10^{-4} \times S + 0.026 \quad (7)$$

where S = salinity. The largest φ_{avg} values were calculated for the SRHA addition to seawater permeate (S = 33.1) and the S = 32.1 surface-water sample from September 2002. These AQYs were not significantly different (unpaired t-test with Welch correction: $p = 0.618$, df = 2).

An analysis of covariance (ANCOVA) between treatments for both surrogates and surface waters was

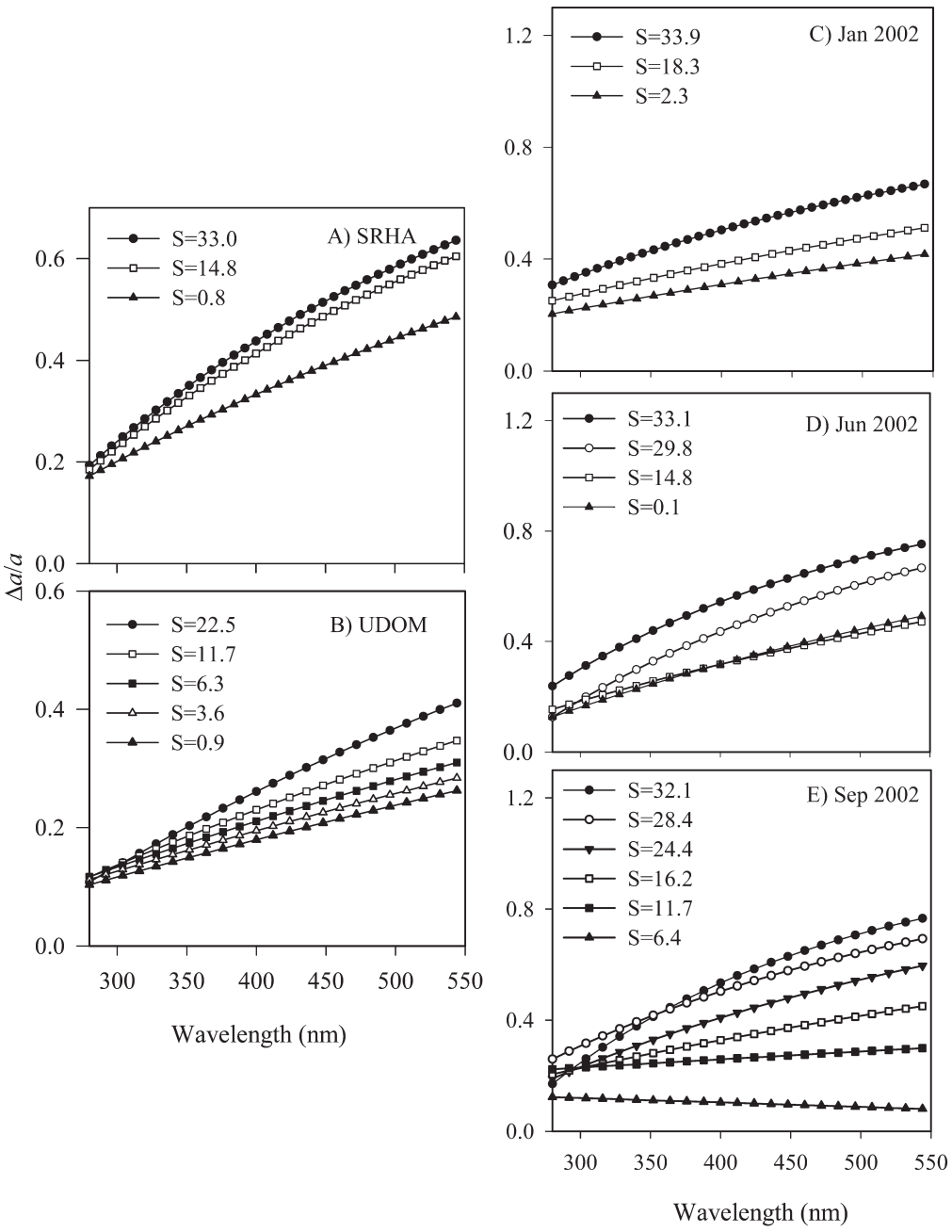

Fig. 4. The relative photobleaching ($\Delta a/a$) after sunlight exposure of (A) SRHA, (B) UDOM, and (C–E) surface-water CDOM plotted as a function of salinity. Each curve represents a different salinity value (S), as indicated.

performed with a Tukey-Kramer posttest ($\alpha = 0.05$, df = 56) to determine significant differences between the linear regression parameters. The linear regression slope coefficients were not significantly different between the surrogate CDOM types and the January 2002 surface-water CDOM type ($p < 0.01$). The regression slope coefficients for the June and September 2002 surface-water CDOM experiments were significantly larger than those for the surrogate CDOM and the January 2002 surface-water experiments ($p < 0.05$), yet were not significantly different from each other ($p < 0.05$). Moreover, significant differences were found between the intercept terms of the regressions.

The SRHA surrogate had the largest intercept value, 0.091 m (mol photons^{-1}), nearly three times larger than the intercept values for the UDOM surrogate (0.029 m [mol photons^{-1}]) and the surface-water CDOM in the CB in 2002, which ranged from 0.010 to 0.039 m (mol photons^{-1}). The intercept for the UDOM surrogate was not significantly different from the intercepts for surface-water CDOM collected in January 2002 and September 2002 ($p > 0.05$). The lowest intercept value, 0.010 m (mol photons^{-1}),

Table 5. Change in AQY for average photobleaching (φ_{avg}) with salinity and linear model results. "UDOM 25%" is the UDOM dilution experiment. SEM was calculated for triplicates. The slope from the regression of all surface waters from 2002 was 20.33×10^{-4} (SEM=2.84).*

Experiment	Salinity	φ_{avg}	SEM	Regression slope	Regression intercept	r^2	p value	F statistic	n
SRHA	33.1	0.118	0.001	8.72×10^{-4}	0.091	0.91	<0.001	69.83	9
	14.1	0.108	0.003						
	0.8	0.089	0.001						
UDOM	22.5	0.041	0.002	5.74×10^{-4}	0.029	0.80	<0.001	50.809	15
	11.7	0.037	0.002						
	6.3	0.035	0.001						
	3.6	0.032	0.002						
	0.9	0.027	0.003						
UDOM 25%	34.0	0.035	0.001	5.31×10^{-4}	0.016	0.98	<0.001	357.32	9
	17.0	0.025	0.001						
	0.1	0.015	0.001						
Jan 2002	33.9	0.070	0.003	7.55×10^{-4}	0.039	0.64	0.01	12.284	9
CDOM	18.3	0.043	0.001						
	2.3	0.046	0.002						
Jun 2002	33.1	0.099	0.003	21.21×10^{-4}	0.010	0.79	<0.001	49.792	12
CDOM	28.9	0.054	0.002						
	13.9	0.029	0.002						
	0.1	0.018	0.001						
Sep 2002	32.1	0.111	0.012	30.11×10^{-4}	0.020	0.86	<0.001	121.82	21
CDOM	28.4	0.118	0.006						
	24.4	0.087	0.001						
	17.1	0.064	0.003						
	16.1	0.075	0.007						
	11.7	0.067	0.007						
	6.4	0.032	0.005						

* UDOM, ultrafiltered river dissolved organic matter; SRHA, Suwannee River humic acid; CDOM, chromophoric dissolved organic matter.

was calculated for the regression from the June 2002 surface-water CDOM, which was significantly different from all other regressions except September 2002.

Dilution of the surrogate CDOM did not appear to change its photoreactivity with respect to salinity. In a separate experiment, 25% of initial UDOM was added to permeate mixtures at salinities of 0.l, 17, and 34. Similar to the undiluted UDOM, φ_{avg} of the 25% dilution increased with salinity (Table 5). The slope of the regression equation for the 25% dilution UDOM was not significantly different from the undiluted UDOM regression slope ($p = 0.62$, df = 17).

Hydrogen peroxide production from UDOM after photobleaching—The production of H_2O_2 was observed in all light-exposed samples of the UDOM surrogate (Table 6). A background H_2O_2 concentration of 4 nmol L^{-1} was measured in all initial and dark control samples and subtracted from light-exposed treatments. Most H_2O_2 production occurred in the first 5 h of the experiment, though H_2O_2 generally increased with the total incubation time of 19 h, spanning 2 d (data not shown). Thus, gross H_2O_2 production rates reported here are in excess of any dark consumption that may have occurred before analysis (O'Sullivan et al. 2005) and production rates are calculated only for the first 5 h of exposure.

The production of H2O2 from UDOM was strongly dependent upon salinity. H_2O_2 production rates from UDOM increased by two orders of magnitude, from 15 to 368 nmol L^{-1} h^{-1}, between freshwater and seawater treatments. The increase in H_2O_2 production exhibited a linear increase with salinity:

$$H_2O_2\left(\text{nmol L}^{-1}\right) = 83.15 \times \text{salinity} - 69.16$$
$$r^2 = 0.99,\ p < 0.001, n = 10. \quad (8)$$

The apparent quantum yields for H_2O_2 photoproduction from UDOM, φ_{hp}, were also calculated for each salinity treatment in the UDOM experiment. The rate of H_2O_2 production was divided by the μmol photons absorbed over the range of 280 to 400 nm (Scully et al. 1996). The values for φ_{hp} increased with salinity from 1.64×10^{-4} to 37.02×10^{-4}.

Discussion

Effects of salinity on the photobleaching of CDOM's spectral properties—The initial light absorption in chromophoric compounds such as lignin occurs near 280 nm, so Δa_{280} might reasonably indicate photochemical degradation of the primary chromophores in CDOM (Del Vecchio and Blough 2004). The fact that Δa_{280} did not change significantly with salinity for either the SRHA or the UDOM experiments suggests that photodegradation of the aromatic chromophores that dominate CDOM absorption

Table 6. Hydrogen peroxide production rates measured after 5 h sunlight exposure of UDOM added to mixtures of freshwater and seawater permeates at various salinities. The apparent quantum yield for H_2O_2 production is also shown as is the starting a_{310} and pH of each UDOM mixture. For standard errors (SEM), n=2 on all measurements.

Salinity	H_2O_2 production (nmol L^{-1} h^{-1})	SEM	φ_{hp} ($\times 10^{-4}$)	Initial a_{310} (m^{-1})	pH
22.5	368	9	37.02	11.76	8.0
11.7	171	13	18.21	11.39	7.8
6.3	74	10	7.82	11.29	7.7
3.6	49	6	5.15	11.34	7.6
0.9	15	1	1.64	11.29	7.6

are not susceptible to changes in salinity, supporting the results of Minor et al (2006). Further, the correlation between Δa_{280} and I_a ($r^2 = 0.76$; Fig. 5A) meant that a_{280} was the best indicator wavelength for monitoring photodegradation of chromophores as a direct result of light absorption.

From our results for both the surrogate and the surface-water CDOM, it was evident that longwave absorption decreased more rapidly than shortwave absorption. Above 280 nm, Δa increased with salinity in both surrogate CDOM experiments (Fig. 2A,B), and $\Delta a/a$ increased both with wavelength and with salinity in the surrogate and surface-water CDOM experiments (Fig. 4). Thus, the increases in photobleaching due to salinity were most pronounced at longer wavelengths, where Del Vecchio and Blough (2002) have also observed more relative photobleaching, and appeared unrelated to the light absorbed by the samples. Neither Δa_{350} nor Δa_{440} were correlated to I_a (Fig. 5B,C) and the effect was most clear when ΔS_g was plotted against I_a (Fig. 6).

Light absorption did not cause the change in S_g values on pooled results. When the surrogate CDOM experimental results and the June 2002 freshwater results were discarded, only 31% of the variation in ΔS_g was explained by the mol photons absorbed m^{-2} (one-way ANOVA, $p < 0.001$, df = 38). Most of the change in S_g should be explained by the quantity of light absorbed, if light absorption was the primary cause of longwave photobleaching. We assert that this 31% represents a statistical effect of primary chromophore degradation on longwave absorption loss (Del Vecchio and Blough 2004), yet the remaining 60% must be due to other factors (e.g., ionic strength or composition from increased salinity).

To produce the observed changes in S_g values, longwave absorption must decrease to a larger degree than shortwave absorption. The changes in $\Delta a/a$ at different wavelengths for the combined surrogate and surface-water CDOM results support this assertion (Fig. 7). We found a poor correlation between $\Delta a/a(280)$ and ΔS_g, yet the correlation improved between comparisons at longer wavelengths. In fact, the best correlation ($r^2 = 0.90$) was found between $\Delta a/a(440)$ and ΔS_g (Fig. 7C). Thus, proportionally more loss in absorption had occurred in the blue-light region relative to the UV region. A similar result was reported for polychromatic irradiation of fulvic acid by Del Vecchio and Blough (2002) and by Grzybowski (2000), who measured faster relative photobleaching at 350 nm compared to 250 nm.

Increases in CDOM apparent quantum yields with salinity—Apparent quantum yields for both photobleaching and for hydrogen peroxide production increased with salinity, indicating higher photoreactivity. Because both CDOM absorption and solar irradiance changed dramatically from 280 to 550 nm, we integrated Δa over that waveband to calculate an averaged apparent quantum yield for photobleaching, φ_{avg} (Moran et al. 2000; Osburn et al. 2001; Tzortziou et al. 2007). The computation of φ_{avg} provided equivalent units in which to compare photobleaching results that might be biased by variations in optical thickness (Hu et al. 2002).

The observed increases in φ_{avg} with salinity for the CDOM surrogates provided the most convincing evidence of an effect of salinity on photobleaching. The increase in φ_{avg} with salinity was also observed in experiments in which the UDOM was diluted to 25% of its initial a_{350} (Table 5). The lack of a significant difference between the regression slopes for the diluted and the undiluted UDOM in the ANCOVA test argues against an effect of optical thickness on the photobleaching results.

Hydrogen peroxide production results from the UDOM surrogate exposure provided additional evidence of an increase in CDOM photoreactivity with salinity. H_2O_2 production from UDOM was not correlated to Δa_{280}, but it was correlated to a_{310} ($r^2 = 0.92$, $n = 10$), similar to humic freshwaters (Scully et al. 1996) and to Δa_{350} ($r^2 = 0.92$, $n = 10$). This result indicates that H_2O_2 production was not coupled to degradation of the primary chromophore.

Further, more H_2O_2 was produced from UDOM as salinity increased, and with greater efficiency (Table 6). The production rates we calculated from UDOM (15–368 nmol L^{-1} h^{-1}) were in the lower range of those reported for freshwater CDOM (81–2120 nmol L^{-1} h^{-1}) by Scully et al. (1996). However, our rates were much larger than H_2O_2 production rates for seawater, which have ranged between 5 and 10 nmol L^{-1} h^{-1} (Yocis et al. 2000; Yuan and Shiller 2001; Gerringa et al. 2004).

Salinity facilitated the efficiency of H_2O_2 production from UDOM. The φ_{hp} value at a salinity of 0.9 was 1.64×10^{-4}, well within the average for humic freshwaters (Scully et al. 1996). When salinity of the UDOM was increased, φ_{hp} increased by a factor of 20, to 37.02×10^{-4}. These results indicated that secondary photochemistry was occurring, because φ_{hp} was highly correlated to φ_{avg} ($r^2 = 0.90$, $p < 0.001$, $n = 10$), even though the increase in φ_{hp} with salinity was much greater than the increase in φ_{avg}. However, the pH did increase from 7.6 to 8.0 in the UDOM experiment, and was the significant predictor of peroxide formation

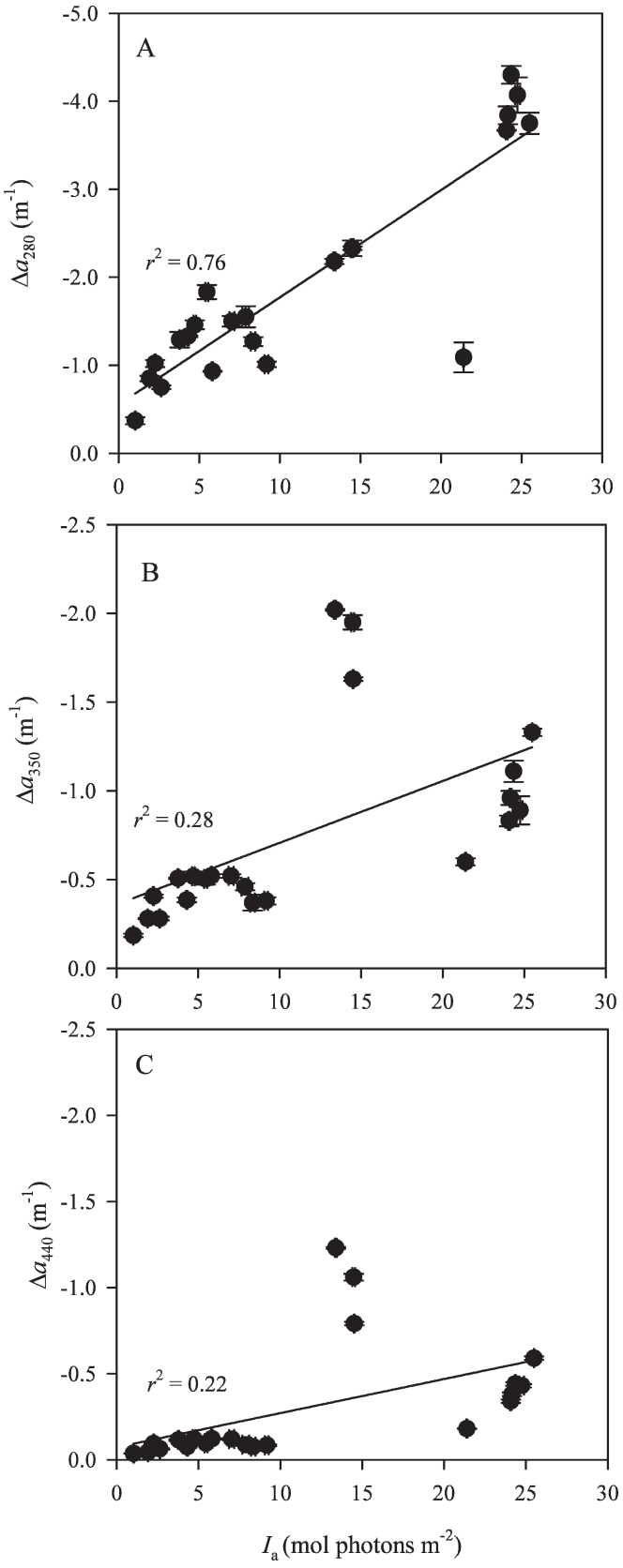

Fig. 5. The photobleaching at specific wavelengths was not always correlated to light absorption, I_a (mol photons m^{-2}). The correlation coefficient decreased for Δa_{350} and Δa_{440}, suggesting a decoupling between initial light absorption and photobleaching at wavelengths >350 nm. Regression statistics were not improved when surrogate and surface-water CDOM results were analyzed separately.

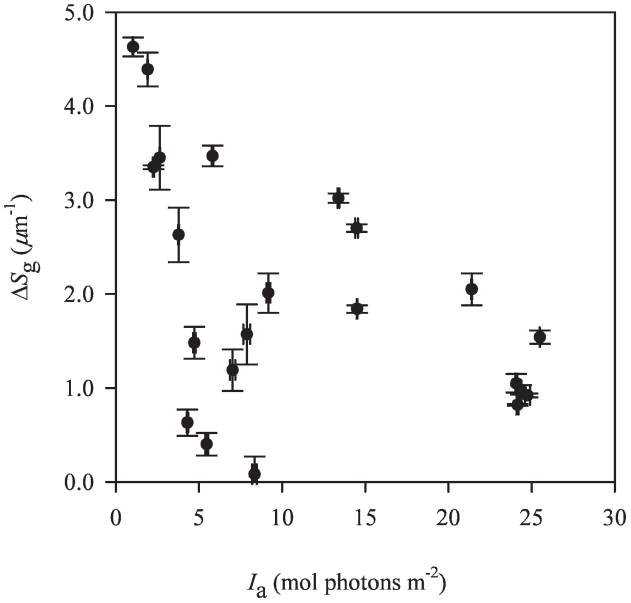

Fig. 6. The change in spectral slope (ΔS_g) as a function of light absorption (I_a).

when considered with Δa_{280} as the index for photodegradation ($r^2 = 0.97$, $F = 58.678$, df = 14, $p = 0.017$).

Contribution of pH and iron to CDOM photobleaching—The pH result raised a concern for our analysis, because both pH and dissolved iron can mediate photochemical reactions in surface waters (Blough and Zepp 1995). If enough Fe(II) is present to be oxidized to Fe(III) from photo-Fenton chemistry, which consumes H_2O_2, OH radical production also could result in CDOM photobleaching (White et al. 2003). At the pH range of our samples (7–8) this process is enhanced and might in part explain the trends in H_2O_2 production we observed during the UDOM photobleaching experiment.

Because we did not measure iron concentrations in our water samples or in the UDOM photobleaching experiment, we constructed a kinetic model based on Siefert et al. (1996) to predict H_2O_2 consumption at pH and iron conditions similar to those of the freshwater location where our UDOM originated. Skrabal (1995) reported that surface-water dissolved iron levels in the CB ranged from 100 to 150 nmol L^{-1} in freshwater to ≤20 nmol L^{-1} at salinities of 18, above which dissolved Fe was below detection. Because the concentration of iron has a much larger influence on H_2O_2 consumption than does the pH, we used concentrations of 500 nmol Fe(III) L^{-1} and 75 nmol Fe(II) L^{-1} to constrain the peroxide consumption as much as possible.

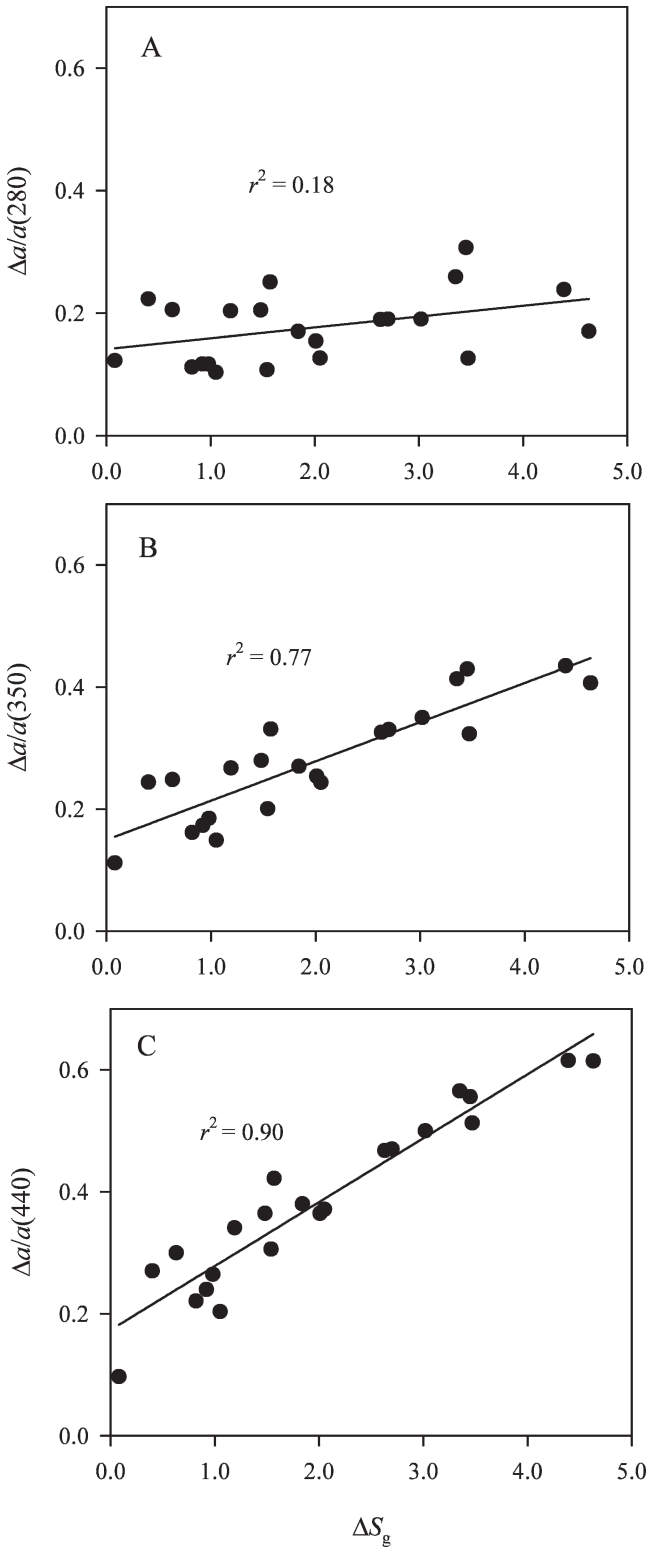

Fig. 7. Relative photobleaching at individual wavelengths vs. the change in S_g values for CDOM exposed to sunlight for 2–3 d. The correlation coefficient was low for (A) shortwave absorption (280 nm) and (B) increased at mid wavelengths (350 nm) into the (C) blue-light absorption band (440 nm).

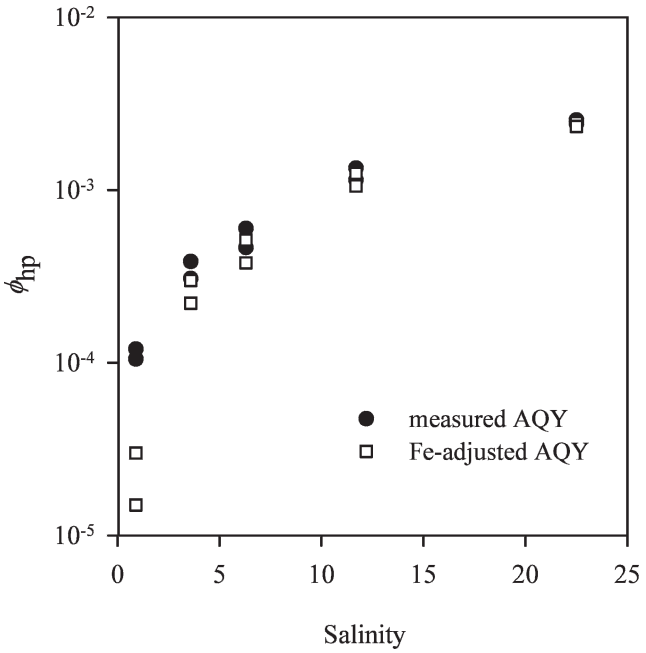

Fig. 8. H_2O_2 production quantum yields (φ_{hp}) from Susquehanna River UDOM as a function of salinity. Closed circles represent the measured experimental results, and open squares represent the values adjusted for pH = 7.0–8.0 and total Fe concentration of 575 nmol L^{-1} as calculated from the kinetic model. *See* text for details of the kinetic model used.

The consumption of H_2O_2 by oxidation of Fe(II) predicted by the model was 40 nmol L^{-1} h^{-1} at pH 7 and 60 nmol L^{-1} h^{-1} at pH 8 with 575 nmol L^{-1} of total iron, an increase of 35%. At the Fe concentrations reported for CB, the model predicted H_2O_2 consumption ranging from 8 to 12 nmol L^{-1}. After values were adjusted to the model-derived H_2O_2 consumption rates, H_2O_2 production still increased with salinity, as did φ_{hp} (Fig. 8). Thus, it seems unlikely that photo-Fenton chemistry consumed enough H_2O_2 to produce the photobleaching results we observed in the UDOM experiment. This effect may be restricted to systems having circumneutral pH where dissolved iron concentrations are relatively low.

Variability of photoreactive CDOM in the CB—The results of the linear regressions between φ_{avg} and salinity in Table 5 provided a context in which to understand the variability in CDOM photoreactivity in the CB. The regression slope coefficients indicated variability with respect to salinity, and the intercepts indicated variability with respect to source in the absence of salinity. The ANCOVA test showed that the SRHA surrogate intercept value was larger than the UDOM surrogate value, probably due to selective differences in humic acid isolation vs. TFF, and the difference in CDOM source between the Suwannee River and the Susquehanna River. Therefore, SRHA was the most photoreactive CDOM in our study because it had the largest intercept value. The surface-water CDOM intercepts overlapped with the UDOM intercept, indicating the similarity between the UDOM and the CDOM from which it was isolated.

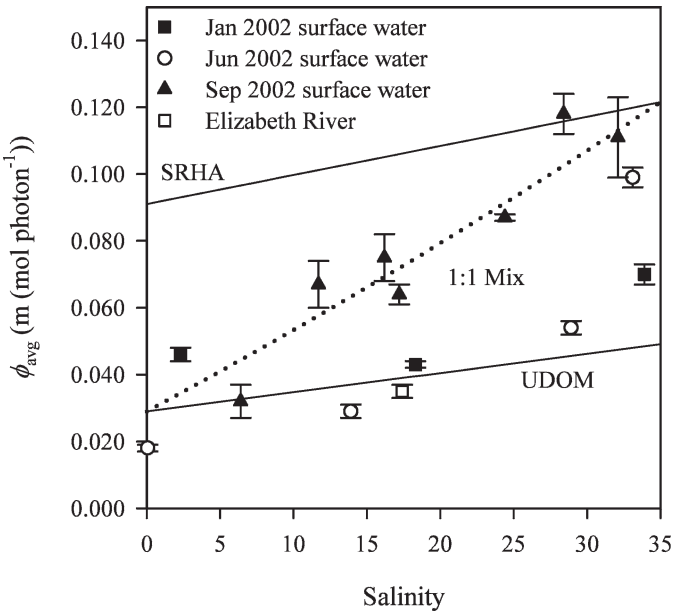

Fig. 9. The changes in CDOM photoreactivity with salinity for the main stem of the CB in 2002 within the modeled changes of CDOM surrogate photoreactivity with salinity. As indicated, the solid lines are CDOM source boundary conditions, which change with salinity based on φ_{avg} calculated for SRHA and UDOM. Individual markers are φ_{avg} values for surface waters from 2002. The dotted line represents the 1 : 1 transition in photoreactivity from UDOM to SRHA based on salinity.

The ANCOVA results demonstrated a similar effect of salinity on CDOM photoreactivity among CDOM sources because the regression slopes increased. However, the June and September 2002 surface-water CDOM regression slopes were significantly greater than the January 2002 and surrogate CDOM regression slopes; yet they were not significantly different from each other. This difference meant that either the source of CDOM or its photoreactivity with respect to salinity changed in the lower CB in 2002.

When φ_{avg} values for the CB in 2002 were plotted against salinity, the trends suggested a change in CDOM source, even when the salinity effect was included (Fig. 9). The solid lines were calculated from the regression models for UDOM (lower bound) and for SRHA (upper bound) from Table 5. A 1 : 1 proportional mix was calculated, assuming that UDOM represented the freshwater reach and SRHA represented the seaward region of the bay. Most of the surface-water CDOM φ_{avg} values from January, June, and September 2002 fell within the two source constraints. As we expected, the lower-salinity surface waters (S = 0–20) were near the UDOM model values. Above a salinity of 20, the surface-water CDOM φ_{avg} values approach the SRHA model values.

An additional φ_{avg} value was calculated for surface-water CDOM from the Elizabeth River collected in September 2002 near Sta. LB (Fig. 1). We included Elizabeth River CDOM because it was similar to the CDOM used in Minor et al (2006). The Elizabeth River φ_{avg} value was closer to the UDOM than the SRHA at a salinity of 17. This result was surprising but might be a function of the higher iron content in Dismal Swamp, which is the source of CDOM for the Elizabeth River (Minor et al. 2006).

The similarity between the riverine UDOM φ_{avg} and surface-water CDOM φ_{avg} at low salinities was not surprising because the Susquehanna River is the main source of freshwater to the upper CB (Schubel and Pritchard 1986). Unexpectedly, φ_{avg} values for surface-water CDOM at salinities >25 were not statistically different from the SRHA treatments ($p = 0.097$; df = 11; $n = 9$; unpaired t-test with Welch correction). The bottom half of the bay is dominated by extensive tidal wetlands and marshes proximal to several rivers (Potomac, Rappahannock, James, York) that have larger DOC concentrations than the Susquehanna River (C. Osburn, unpubl.), and prior work has shown that marshes can export highly photoreactive CDOM (Tzortziou et al. 2007).

A change in CDOM source seems most likely. The difference between the UDOM φ_{avg} at low salinity and the SRHA φ_{avg} at high salinity plotted in Fig. 9 produced a slope coefficient of 28.26×10^{-4}, within the range of the June and September 2002 CDOM slope coefficients. This analysis suggests a switch in CDOM source from the upper CB, dominated by the Susquehanna River, to DOM in the lower CB, dominated by coastal wetlands and more humic rivers that drain the Atlantic coastal plain. Even so, the slope coefficient calculated for the switch in CDOM source was a function of the changing φ_{avg} with salinity for each surrogate.

In conclusion, longwave photobleaching of CDOM increased with salinity both for surrogates of CDOM and for surface waters of the CB. These results demonstrate the importance of coastal mixing of photoreactive freshwater with high ionic strength seawater to the increased transparency of surface waters in the coastal ocean. Intramolecular photochemistry may be the cause of longwave photobleaching responsible for the measured photoreactivity, because it appeared uncoupled from primary chromophore degradation due to light absorption. Further, the disproportionately greater photobleaching observed at wavelengths above 400 nm complicates their use as tracers of terrigenous organic matter. Primarily, this is because DOC concentration may be uncoupled from CDOM light absorption at wavelengths such as 440 nm due to photobleaching under the conditions we described here. The implication is that longwave CDOM absorption is not always conservative.

References

Blough, N. V., and R. G. Zepp. 1995. Reactive oxygen species in natural waters, p. 280–333. *In* C. S. Foote, J. S. Valentine, A. Greenberg and J. F. Liebman [eds.], Active oxygen: Reactive oxygen species in chemistry. Chapman and Hall.

Boyd, T. J., and C. L. Osburn. 2004. Changes in CDOM fluorescence from allochthonous and autochthonous sources during tidal mixing and bacterial degradation in two coastal estuaries. Mar. Chem. **89:** 189–210.

Del Vecchio, R., and N. V. Blough. 2002. Photobleaching of chromophoric dissolved organic matter in natural waters: Kinetics and modeling, Mar. Chem. **78:** 231–253.

———, AND ———. 2004. On the origin of the optical properties of humic substances. Environ. Sci. Technol. **38:** 3885–3891.

GAO, H. Z., AND R. G. ZEPP. 1998. Factors influencing photoreactions of dissolved organic matter in a coastal river of the southeastern United States. Environ. Sci. Technol. **32:** 2940–2946.

GERRINGA, L. J. A., M. J. A. RIJKENBERG, K. R. TIMMERMANS, AND A. G. J. BUMA. 2004. The influence of solar ultraviolet radiation on the photochemical production of H_2O_2 in the equatorial Atlantic Ocean. J. Sea Res. **51:** 3–10.

GOLDSTONE, J. V., R. DEL VECCHIO, N. V. BLOUGH, AND B. M. VOELKER. 2004. A multicomponent model of chromophoric dissolved organic matter photobleaching. Photochem. Photobiol. **80:** 52–60.

GRYZYBOWSKI, W. 2000. Effect of short-term sunlight irradiation on absorbance spectra of chromophoric organic matter dissolved in coastal and riverine water. Chemosphere **40:** 1313–1318.

HU, C., F. E. MULLER-KARGER, AND R. G. ZEPP. 2002. Absorbance, absorption coefficient, and apparent quantum yield: A comment on common ambiguity in the use of these optical concepts. Limnol. Oceanogr. **47:** 1261–1267.

KORSHIN, G. V., C.-W. LI, AND M. BENJAMIN. 1997. Monitoring the properties of natural organic matter through UV spectroscopy: A consistent theory. Water Res. **31:** 1787–1795.

LEE, M., D. O'SULLIVAN, K. B. NOONE, AND B. G. HEIKES. 1995. HPLC method for the determination of H_2O_2, C_1 and C_2 hydroperoxides in the atmosphere. J. Atmos. Ocean. Technol. **12:** 1060–1070.

MILLER, W. L. 1998. Effects of UV radiation on aquatic humus: Photochemical principles and experimental considerations, p. 125–141. *In* D. O. Hessen and L. J. Tranvik [eds.], Aquatic humic substances: Ecology and biogeochemistry. Ecological studies. Springer.

———, AND R. G. ZEPP. 1995. Photochemical production of dissolved inorganic carbon from terrestrial organic matter: Significance to the oceanic organic carbon cycle. Geophys. Res. Lett. **22:** 417–420.

MINOR, E. C., J. POTHEN, B. J. DALZELL, H. ABDULLA, AND K. MOPPER. 2006. Effects of salinity changes on the photodegradation and ultraviolet-visible absorbance of terrestrial dissolved organic matter. Limnol. Oceanogr. **51:** 2181–2186.

MORAN, M. A., W. M. SHELDON, AND R. G. ZEPP. 2000. Carbon loss and optical property changes during long-term photochemical and biological degradation of estuarine dissolved organic matter. Limnol. Oceanogr. **45:** 1254–1264.

MORRIS, D. P., AND B. R. HARGREAVES. 1997. The role of photochemical degradation of dissolved organic carbon in regulating the UV transparency of three lakes on the Pocono Plateau. Limnol. Oceanogr. **42:** 239–249.

NEALE, P. J., AND D. J. KIEBER. 2000. Assessing biological and chemical effects of UV in the marine environment: Spectral weighting functions, p. 61–83. *In* R. E. Hester and R. M. Harrison [eds.], Causes and environmental implications of increased U.V.-B radiation. Issues in environmental science and technology. Royal Society of Chemistry.

OSBURN, C. L., AND D. P. MORRIS. 2003. Photochemistry of chromophoric dissolved organic matter in natural waters, p. 187–217. *In* E. W. Hebling and H. Zagarese [eds.], UV effects in aquatic organisms and ecosystems. Royal Society of Chemistry.

———, H. E. ZAGARESE, D. P. MORRIS, B. R. HARGREAVES, AND W. E. CRAVERO. 2001. Calculation of spectral weighting functions for the solar photobleaching of chromophoric dissolved organic matter in temperate lakes. Limnol. Oceanogr. **46:** 1455–1467.

O'SULLIVAN, D. W., P. J. NEALE, R. B. COFFIN, T. J. BOYD, AND C. L. OSBURN. 2005. Photochemical production of hydrogen peroxide and methylhydroperoxide in coastal waters. Mar. Chem. **97:** 14–33.

SCHUBEL, J. R., AND D. W. PRITCHARD. 1986. Responses of upper Chesapeake Bay to variations in discharge of the Susquehanna River. Estuaries **9:** 236–249.

SCULLY, N. M., D. J. MCQUEEN, D. R. S. LEAN, AND W. J. COOPER. 1996. Hydrogen peroxide formation: The interaction of ultraviolet radiation and dissolved organic carbon in lake waters along a 43–75 degrees N gradient. Limnol. Oceanogr. **41:** 540–548.

SIEFERT, R. L., S. M. WEBB, AND M. R. HOFFMAN. 1996. Determination of photochemically available iron in ambient aerosols. J. Geophys. Res. **101:** 14441–14449.

SKRABAL, S. A. 1995. Distributions of dissolved titanium in Chesapeake Bay and the Amazon River Estuary. Geochim. Cosmochim. Acta **59:** 2449–2458.

STEDMON, C. A., S. MARKAGER, AND H. KAAS. 2000. Optical properties and signatures of chromophoric dissolved organic matter (CDOM) in Danish coastal waters. Estuar. Coast. Shelf Sci. **51:** 267–278.

SUTTON, R., AND G. SPOSITO. 2005. Molecular structure in soil humic substances: The new view. Environ. Sci. Technol. **39:** 9009–9015.

TZORTZIOU, M., C. L. OSBURN, AND P. J. NEALE. 2007. Photobleaching of dissolved organic material from a tidal marsh-estuarine system of the Chesapeake Bay. Photochem. Photobiol. **83:** 782–792.

VODACEK, A., N. V. BLOUGH, M. D. DEGRANDPRE, E. T. PELTZER, AND R. K. NELSON. 1997. Seasonal variation of CDOM and DOC in the Middle Atlantic Bight: Terrestrial inputs and photooxidation. Limnol. Oceanogr. **42:** 674–686.

WHITE, E. M., P. P. VAUGHAN, AND R. G. ZEPP. 2003. Role of photo-Fenton reaction in the production of hydroxyl radicals and photobleaching of colored dissolved organic matter in a coastal river of the southeastern United States. Aquat. Sci. **65:** 402–414.

YOCIS, B. H., D. J. KIEBER, AND K. MOPPER. 2000. Photochemical production of hydrogen peroxide in Antarctic waters. Deep-Sea Res. I **47:** 1077–1099.

YUAN, J., AND A. M. SHILLER. 2001. The distribution of hydrogen peroxide in the southern and central Atlantic Ocean. Deep-Sea Res. II **48:** 2947–2970.

ZEPP, R. G. 1988. Environmental photoprocesses involving natural organic matter, p. 193–214. *In* F. H. Frimmel and R. F. Christman [eds.], Humic substances and their role in the environment. Wiley.

Edited by: Elizabeth A. Canuel

Received: 19 December 2007
Accepted: 22 July 2008
Amended: 08 September 2008